Soft Matter

PAPER

Cite this: *Soft Matter*, 2015, **11**, 1087

Synthesis, characterization, and tuning of the liquid crystal properties of ionic materials based on the cyclic polyoxothiometalate $[\{Mo_4O_4S_4(H_2O)_3(OH)_2\}_2(P_8W_{48}O_{184})]^{36-}$†

Nancy Watfa,[abc] Sébastien Floquet,*[ad] Emmanuel Terazzi,*[e] Mohamed Haouas,*[a] William Salomon,[a] Vladimir S. Korenev,[afg] Francis Taulelle,[a] Laure Guénée,[e] Akram Hijazi,[bc] Daoud Naoufal,[bc] Claude Piguet[e] and Emmanuel Cadot[a]

Received 18th November 2014
Accepted 11th December 2014

DOI: 10.1039/c4sm02551b

www.rsc.org/softmatter

A series of compounds resulting from the ionic association of a nanoscopic inorganic cluster of formula $[K_2Na_xLi_y\{Mo_4O_4S_4(OH)_2(H_2O)_3\}_2(H_zP_8W_{48}O_{184})]^{(34-x-y-z)-}$, **1**, with several organic cations such as dimethyldioctadecylammonium $DODA^+$, trimethylhexadecylammonium $TMAC_{16}^+$, alkylmethylimidazoliums $mimC_n^+$ (n = 12–20) and alkyl-dimethylimidazoliums $dmimC_n^+$ (n = 12 and 16) was prepared and characterized in the solid state by FT-IR, EDX, Elemental analysis, TGA and solid state NMR. The solid state NMR experiments performed on ^1H, ^{13}C and ^{31}P nuclei evidenced the interactions between the cations and **1** as well as the organization of the alkyl chains of the cations within the solid. Polarized optical microscopy, DSC and SA-XRD experiments implicated mesomorphic phases for $DODA^+$ and $mimC_n^+$ salts of **1**. The crystallographic parameters were determined and demonstrated that the inter-lamellar spacing could be controlled upon changing the length of the alkyl chain, a very interesting result if we consider the huge size of the inorganic cluster **1** and the simple nature of the cations.

Introduction

Polyoxometalates (POMs) are often described as metal–oxide clusters with structural, electronic and functional versatility. Much current activity in POMs chemistry is driven by potential applications in catalysis,[1,2] electrocatalysis,[3] medicine,[4] magnetism,[5] materials sciences and nanotechnology.[6,7] Liquid crystals constitute a fascinating example of functional self-assembled materials, and the incorporation of some inorganic components into liquid crystalline phases appears particularly relevant to the elaboration of synergistic multifunctional materials.[8,9] A large part of the metallomesogens is prepared by chemical integration of metal ions into organic ligands, which offers a large panel of materials tuned by the design of the organic part.[10–15] Another approach consists in pairing inorganic clusters with organic cations possessing long alkyl chains and bearing mesogenic functions. Using this strategy, Molard *et al.* combined the cluster $[Re_6Se_8(CN)_6]^{n-}$ (n = 3 and 4) with tetraalkylammonium cations functionalized with cyanobiphenyl groups to design clustomesogens possessing switchable magnetic/luminescence properties.[16] In the field of heteropolyoxometalates (POM), Wu *et al.* succeeded in designing a number of POM-based ionic liquid crystals with the help of organic cations bearing aromatic groups.[17–23]

In this context, we recently reported that the association of the keplerate nanocapsules $[Mo_{132}O_{372}(CH_3COO)_{30}(H_2O)_{72}]^{42-}$ and $[Mo_{132}S_{60}O_{312}(SO_4)_n(H_2O)_{132-2n}]^{(12+2n)-}$ (n = 23 or 30) with dioctadecyl-dimethylammonium cations ($DODA^+$) gave ionic materials exhibiting liquid crystal properties at room temperature.[24,25] Interestingly, even if the keplerate clusters are perfectly spherical, the $DODA^+$ cations are not randomly distributed around the clusters. These results prompted us to extend our

[a]*Institut Lavoisier de Versailles, UMR 8180, University of Versailles, 45 Avenue des Etats-Unis, 78035 Versailles, France. E-mail: sebastien.floquet@uvsq.fr; mohamed.haouas@uvsq.fr*

[b]*Laboratoire de Chimie de Coordination Inorganique et Organométallique LCIO, Université Libanaise, Faculté des Sciences I, Hadath, Lebanon*

[c]*Ecole Doctorale des Sciences et Technologie EDST, PRASE, Université Libanaise, Lebanon*

[d]*Institut Universitaire de France, 103 boulevard Saint-Michel 75005, Paris, France*

[e]*Department of Inorganic and Analytical Chemistry, University of Geneva, 30 quai E. Ansermet, CH-1211 Geneva 4, Switzerland. E-mail: Emmanuel.Terazzi@unige.ch*

[f]*Nikolaev Institute of Inorganic Chemistry, SB RAS, Novosibirsk 630090, Russia*

[g]*Novosibirsk State University, Novosibirsk, Russia 630090*

† Electronic supplementary information (ESI) available: FT-IR spectra of starting salts of cations compared to those of POM-based materials (Fig. S1–S9); FT-IR spectra recorded in the 20–300 °C temperature range for selected materials (Fig. S10–S12); TGA traces of POM-based materials (Fig. S13–S21); ^1H NMR spectra of some POM-based materials in $CDCl_3$ compared with the corresponding organic cations alone (Fig. S22–S24); ^{31}P NMR spectra in aqueous solution of **1** associated to different alkali metals (Fig. S25); additional solid state NMR spectra (Fig. S26–S30); additional SA-XRD patterns recorded at 200 °C (Fig. S31–S35); indexation of SA-XRD patterns of the liquid crystalline compounds in 40–200 °C range (Tables S1–S6). See DOI: 10.1039/c4sm02551b

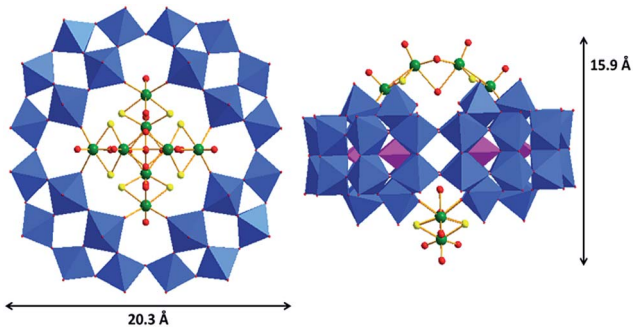

Fig. 1 Top and side structural views of the perpendicular isomer of **1** in polyhedral and ball-and-stick representation. The $\{P_8W_{48}\}$ moiety is depicted in blue and pink polyhedra, molybdenum in green, sulfur in yellow and oxygen in red.

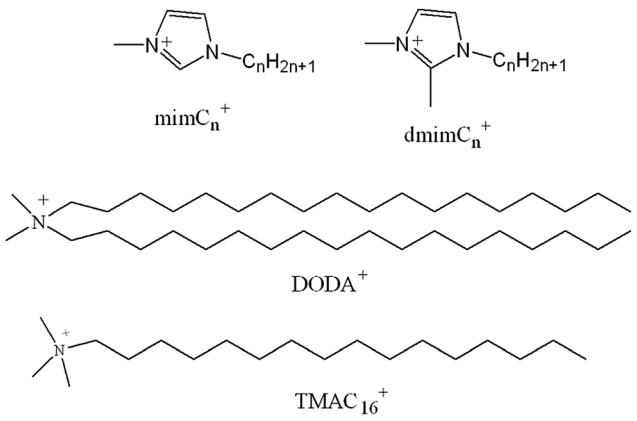

Scheme 1 Cations used in this study.

investigation toward other highly charged polyoxometalate systems exhibiting shape anisotropy. The cyclic superlacunary anionic POM $[H_7P_8W_{48}O_{184}]^{33-}$ (P_8W_{48})[26] represents an attractive system. It possesses a large anionic pocket of about 1 nm in diameter, which is able to include various transition metals, a key step for the elaboration of efficient materials for magnetic, luminescent, catalytic or electrocatalytic properties.[27,28] Consequently this system offers the possibility to design multifunctional materials by association with appropriate organic cations. Additionally, this macrocyclic system could offer promising properties towards the sequestration of various substrates or for catalysis as highlighted by Noro, Cronin and Nakamura with the encapsulation of the gigantic ring-shape cluster $[Mo_{154}(NO)_{14}O_{448}H_{14}(H_2O)_{70}]^{28-}$ with $DODA^+$ cations.[29,30] Herein, we report on the preparation, the characterization in the solid state and the properties of POM-based ionic liquid crystal materials obtained by the electrostatic combination of a ring-shape polyoxothiometalate $[\{Mo_4O_4S_4(H_2O)_3(OH)_2\}_2(P_8W_{48}O_{184})]^{36-}$ (Fig. 1)[31] with various organic cations depicted in Scheme 1. These latter correspond to simple tetraalkylammonium and imidazolium salts, which are commercially available or easily prepared, thus offering the possibility to prepare these materials on a large scale.

Experimental section

Physical methods

Fourier transformed infrared (FT-IR) spectra. Fourier Transformed Infrared (FT-IR) spectra were recorded on a 6700 FT-IR Nicolet spectrophotometer, using diamond ATR technique. The spectra were recorded on undiluted samples and ATR correction was applied. The variable temperature FT-IR spectra were recorded on an IRTF Nicolet iS10 spectrometer in diffuse reflectance mode by using high temperature diffuse reflectance environmental chamber. The background was recorded using dry KBr at 150 °C and the samples were diluted into a KBr matrix (about 10% of compound) before heating. The FT-IR spectra were recorded in the 20–300 °C temperature range under air with a heating rate of 2 °C min^{-1}. Elemental analyses were performed by the service central d'analyses du CNRS, Vernaison, France and by the service d'analyses du CNRS, ICSN, Gif sur Yvette, France. Water content was determined by thermal gravimetric (TGA) analysis with a Seiko TG/DTA 320 thermogravimetric balance (5 °C min^{-1}, under O_2). Energy-dispersive X-ray spectroscopy (EDX) measurements were performed on a JEOL JSM 5800LV apparatus.

Nuclear magnetic resonance (NMR). Solution ^{1}H NMR measurements were performed on a Bruker Avance 300 instrument operating at 300 MHz in 5 mm o.d. tubes. Chemical shifts were referenced to TMS. Solid-state NMR spectra were measured at room temperature under magic angle spinning (MAS) condition. The NMR spectra were obtained on a Bruker Avance-500 spectrometer equipped with a MAS accessory operating at 500.125, 125.761, and 202.452 MHz for ^{1}H, ^{13}C and ^{31}P. Zirconium oxide cylindrical-type rotors (3.2 mm outer diameter) were used. ^{1}H NMR spectra were recorded with single 90° pulse (3.8 μs) at spinning rate of about 20 kHz. The spectral width and data points were 10 kHz and 1000 respectively. The spectra were obtained after 8 transients at a repetition time of *ca.* 30 s. ^{31}P$\{^1$H$\}$ and ^{13}C$\{^1$H$\}$ CPMAS NMR spectra were recorded with typical rf field in X channel (^{13}C or ^{31}P) of *ca.* 90 kHz, high power decoupling during acquisition (26 ms) of *ca.* 50–60 kHz, and contact time of 1–2 ms. 2D ^{1}H → ^{31}P MAS heteronuclear correlation (HETCOR) experiments were performed using CP transfer. The chemical shifts were calibrated relative to a 85% H_3PO_4 solution (set to $\delta = 0$ ppm) for ^{31}P, and adamantane (set to $\delta = 1.74$ ppm in ^{1}H and 38.48 ppm in ^{13}C with respect to TMS) for ^{1}H and ^{13}C as external standards. The experimental errors on the chemical shifts were estimated to be ±0.4 ppm.

Differential scanning calorimetry (DSC). DSC traces were obtained with a Mettler Toledo DSC1 Star Systems differential scanning calorimeter from 3 to 5 mg samples (5 °C min^{-1}, under N_2). Several thermal cycles were performed between −40 °C and 220 °C, the first one allowing the removal of water and the relaxation of the solid, the following cycles explored the reproducibility and the thermal stability of the materials in this temperature range.

Temperature dependent polarized optical microscopy (TD-POM). Temperature dependent polarized optical microscopy (TD-POM) characterizations of the optical textures of the

mesophases were performed with a Leitz Orthoplan Pol polarizing microscope with a Leitz LL 20×/0.40 polarizing objective and equipped with a Linkam THMS 600 variable temperature stage.

Small angle X-ray diffraction (SA-XRD). The crude powder was filled in Lindemann capillaries of 0.8 mm diameter. Diffraction patterns were measured with a STOE transmission powder diffractometer system STADI P using a focused monochromatic Cu-Kα1 beam obtained from a curved Germanium monochromator (Johann-type) and collected on a curved image plate position-sensitive detector (IP-PSD). A calibration with silicon and copper laurate standards, for high and low angle domains, respectively, was preliminarily performed. Sample capillaries were placed in the high-temperature furnace for measurements in the range of desired temperatures (from −40 up to 240 °C) within 0.05 °C. Periodicities up to 50 Å could be measured. The exposure times were of 15 min. For compound **(mimC$_{16}$)$_{23}$–1**, X-ray diffraction experiments were performed on an Empyrean (PANalytical) diffractometer in capillary mode, with a focusing X-ray mirror for Cu radiation and a PIXcel3D area detector.

Syntheses

The precursor $Na_{25}Li[K_2\{Mo_4O_4S_4(OH)_2(H_2O)_3\}_2(H_8P_8W_{48}O_{184})]\cdot 125H_2O$, noted **NaK–1**, was prepared according to the literature and characterized by standard methods.[31] Trimethylhexadecylammonium chloride and dimethyldioctadecylammonium chloride were purchased from Aldrich or Acros chemicals.

Synthesis of 1-methyl-3-alkylimidazolium bromides, mimC$_n$Br (n = 12, 14, 16, 18, 20). 10^{-2} mole of 1-methyl imidazole and 1.2 × 10^{-2} mole of $C_nH_{2n+1}Br$ were dissolved in acetonitrile (5 mL for n = 12–16, 15 mL for n = 18 and 20). The resulting solution was refluxed for 24 h. After, cooling in an ice bath; a precipitate appeared. The latter was isolated by filtration and washed with diethyl ether. The **mimC$_n$Br** salts were characterized by FT-IR and ^{1}H NMR in $CDCl_3$ (see ESI†).

Synthesis of 1,2-dimethyl-3-alkylimidazolium bromides, dmimC$_n$Br (n = 12 and 16). The same procedure was used except that 10^{-2} mole of 1,2-dimethylimidazole was used. The **dmimC$_n$Br** salts were characterized by FT-IR and ^{1}H NMR in $CDCl_3$ (see ESI†).

Synthesis of POM-based materials

The POM-based materials presented in this study were prepared by phase transfer of the anionic cluster **1** from aqueous LiCl 1 M solution into chloroform. 300 mg of the precursor **NaK–1** (0.018 mmol) were solubilised in aqueous LiCl 1 M solution (30 mL). The resulting red solution was then added to a chloroform solution containing a large excess of the organic cation (150 equivalents per **NaK–1**, 2.7 mmol). After vigorous stirring for one hour, the cluster **1** was totally transferred into the organic phase, which was separated from the colourless aqueous phase. Addition of ethanol into the organic phase induced the formation of a red-orange solid, which was isolated by filtration, washed with ethanol and dried in air.

$(DODA)_{19}[K_2Na_2Li_5\{Mo_4O_4S_4(OH)_2(H_2O)_3\}_2(H_8P_8W_{48}O_{184})]\cdot 10H_2O$, DODA$_{19}$–1. $(DODA)_{19}[K_2Na_2Li_5\{Mo_4O_4S_4(OH)_2(H_2O)_3\}_2(H_8P_8W_{48}O_{184})]\cdot 10H_2O$, **DODA$_{19}$–1** was prepared by using 1.56 g of dimethyldioctadecylammonium chloride **DODACl** (2.68 mmol). Yield 421 mg, 94%. IR/cm^{-1}: 2954 (m), 2920 (vs), 2870 (m), 2851 (s), 1639 (mw), 1467 (m), 1135 (m), 1078 (m), 1022 (w), 939 (s), 879 (m), 792 (s), 723 (s). Elemental analysis calcd (%) for $(DODA)_{19}[K_2Na_2Li_5H_8P_8W_{48}O_{184}Mo_8O_8S_8(OH)_4(H_2O)_6]\cdot 10H_2O$ (M = 24 143.3 g nmol^{-1}) Li 0.14; Na 0.19; K 0.32; C 35.92; H 6.52; N 1.10; S 1.06. Found: Li 0.12; Na 0.16; K 0.21; C 35.82; H 6.36; N 1.29; S 0.95. EDX atomic ratios calculated for $(DODA)_{19}[K_2Na_2Li_5H_8P_8W_{48}O_{184}Mo_8O_8S_8(OH)_4(H_2O)_6]\cdot 10H_2O$ (found): Mo/S = 1 (1.10); W/Mo = 6 (5.87); W/P = 6 (6.05); Na/K = 1 (1.15). TGA: a weight loss of 1.1% between RT and 150 °C corresponding to crystallization and coordinated water molecules (calcd: 1.2%).

$(NMe_3C_{16}H_{33})_{18}[K_2Na_2Li_6\{Mo_4O_4S_4(OH)_2(H_2O)_3\}_2(H_8P_8W_{48}O_{184})]\cdot 30H_2O$, $(TMAC_{16})_{18}$–1. $(NMe_3C_{16}H_{33})_{18}[K_2Na_2Li_6\{Mo_4O_4S_4(OH)_2(H_2O)_3\}_2(H_8P_8W_{48}O_{184})]\cdot 30H_2O$, **$(TMAC_{16})_{18}$–1** was prepared by using 860 mg of trimethylhexadecylammonium chloride (2.68 mmol). Yield 295 mg, 85%. IR/cm^{-1}: 2954 (m), 2924 (vs), 2871 (m), 2853 (s), 1636 (mw), 1487 (m), 1474 (m), 1469 (m), 1130 (ms), 1076 (m), 1022 (w), 941 (s), 879 (m, sh.), 794 (s), 722 (s). Elemental analysis calcd (%) for $(N(Me)_3C_{16})_{18}[K_2Na_2Li_6H_8P_8W_{48}O_{184}Mo_8O_8S_8(OH)_4(H_2O)_6]\cdot 30H_2O$ (M = 19 180.4 g mol^{-1}) Li 0.22; Na 0.23; C 21.42; H 4.41; N 1.31; S 1.34. Found: Li 0.24; Na 0.13; C 21.20; H 4.36; N 1.09; S 1.20. EDX atomic ratios calculated for $(N(Me)_3C_{16})_{18}[K_2Na_2Li_6H_8P_8W_{48}O_{184}Mo_8O_8S_8(OH)_4(H_2O)_6]\cdot 30H_2O$ (found): Mo/S = 1 (1.15); W/Mo = 6 (6.22); W/P = 6 (5.82); Na/K = 1 (1.06). TGA: a weight loss of 3.1% between RT and 180 °C corresponding to crystallization and coordinated water molecules (calcd: 3.4%).

$(mimC_{12}H_{25})_{25}[K_2NaLi_4\{Mo_4O_4S_4(OH)_2(H_2O)_3\}_2(H_4P_8W_{48}O_{184})]\cdot 20H_2O$, $(mimC_{12})_{25}$–1. $(mimC_{12}H_{25})_{25}[K_2NaLi_4\{Mo_4O_4S_4(OH)_2(H_2O)_3\}_2(H_4P_8W_{48}O_{184})]\cdot 20H_2O$, **$(mimC_{12})_{25}$–1** was prepared by using $mimC_{12}Br$ (890 mg, 2.68 mmol). Yield 341 mg, 95%. IR/cm^{-1}: 3144 (m), 3101 (m), 3080 (m), 2956 (m), 2925 (vs), 2870 (m), 2854 (s), 1631 (mw), 1571 (m), 1466 (m), 1166 (m), 1131 (m), 1077 (m), 1021 (w), 941 (s), 887 (m), 818 (s), 744 (vs). Elemental analysis calcd (%) for $(mimC_{12}H_{25})_{25}[K_2NaLi_4H_4P_8W_{48}O_{184}Mo_8O_8S_8(OH)_4(H_2O)_6]\cdot 20H_2O$ (M = 20 123.3 g mol^{-1}) Li 0.14; Na 0.12; C 24.09; H 4.12; N 3.51; S 1.29. Found: Li 0.14; Na 0.11; C 23.87; H 4.18; N 3.48; S 1.27. EDX atomic ratios calculated for $(mimC_{12}H_{25})_{25}[K_2NaLi_4H_4P_8W_{48}O_{184}Mo_8O_8S_8(OH)_4(H_2O)_6]\cdot 20H_2O$ (found): Mo/S = 1 (0.91); W/Mo = 6 (5.85); W/P = 6 (6.34); Na/K = 0.50 (0.79). TGA: a weight loss of 2.3% between RT and 180 °C corresponding to crystallization and coordinated water molecules (calcd: 2.3%).

$(mimC_{14}H_{29})_{26}[K_2Na_2Li_3\{Mo_4O_4S_4(OH)_2(H_2O)_3\}_2(H_3P_8W_{48}O_{184})]\cdot 35H_2O$, $(mimC_{14})_{26}$–1. $(mimC_{14}H_{29})_{26}[K_2Na_2Li_3\{Mo_4O_4S_4(OH)_2(H_2O)_3\}_2(H_3P_8W_{48}O_{184})]\cdot 35H_2O$, **$(mimC_{14})_{26}$–1** was prepared by using aqueous LiCl 1 M solution and $mimC_{14}Br$ (960 mg, 2.68 mmol). Yield 220 mg, 59%. IR/cm^{-1}: 3144 (m), 3091 (m), 3074 (m), 2955 (m), 2920 (vs), 2871 (m), 2851 (s), 1636 (mw), 1572 (m), 1467 (m), 1168 (m), 1130 (m), 1077 (m), 1020 (w), 936 (s), 882 (mw), 802 (s), 733 (vs). Elemental analysis calcd (%) for $(mimC_{14}H_{29})_{26}[K_2Na_2Li_3H_3P_8W_{48}O_{184}Mo_8O_8S_8(OH)_4(H_2O)_6]\cdot$

$35H_2O$ (M = 21 389.4 g mol^{-1}) Li 0.10; Na 0.22; C 26.28; H 4.70; N 3.40; S 1.20. Found: Li 0.22; Na 0.35; C 26.57; H 4.53; N 3.58; S 1.12. EDX atomic ratios calculated for $(mimC_{14}H_{29})_{26}[K_2Na_2Li_3H_3P_8W_{48}O_{184}Mo_8O_8S_8(OH)_4(H_2O)_6]\cdot 35H_2O$ (found): Mo/S = 1 (1.09); W/Mo = 6 (6.07); W/P = 6 (6.02); Na/K = 1 (1.28). TGA: a weight loss of 3.4% between *RT* and 170 °C corresponding to crystallization and coordinated water molecules (calcd: 3.5%).

$(mimC_{16}H_{33})_{23}[K_2Na_3Li_3\{Mo_4O_4S_4(OH)_2(H_2O)_3\}_2(H_5P_8W_{48}O_{184})]\cdot 40H_2O$, $(mimC_{16})_{23}$–1. $(mimC_{16}H_{33})_{23}[K_2Na_3Li_3\{Mo_4O_4S_4(OH)_2(H_2O)_3\}_2(H_5P_8W_{48}O_{184})]\cdot 40H_2O$, **$(mimC_{16})_{23}$–1** was prepared by using $mimC_{16}Br$ (1.038 g, 2.68 mmol). Yield 218 mg, 59%. IR/cm^{-1}: 3144 (m), 3102 (m), 3075 (m), 2955 (m), 2922 (vs), 2871 (m), 2852 (s), 1637 (mw), 1571 (m), 1467 (m), 1166 (m), 1136 (m), 1078 (m), 1016 (w), 932 (s), 880 (mw), 799 (s), 721 (vs). Elemental analysis calcd (%) for $(mimC_{16}H_{33})_{23}[K_2Na_3Li_3\ H_5P_8W_{48}O_{184}Mo_8O_8S_8(OH)_4\ (H_2O)_6]\cdot 40H_2O$ (M = 21 311.2 g mol^{-1}) C 25.93; H 4.72; N 3.02; S 1.20. Found: C 26.09; H 4.62; N 3.18; S 1.33. EDX atomic ratios calculated for $(mimC_{16}H_{33})_{23}[K_2Na_3Li_3H_5P_8W_{48}O_{184}Mo_8O_8S_8\ (OH)_4(H_2O)_6]\cdot 40H_2O$ (found): Mo/S = 1 (1.02); W/Mo = 6 (5.73); W/P = 6 (5.58); Na/K = 1.5 (1.65). TGA: a weight loss of 4.1% between *RT* and 170 °C corresponding to crystallization and coordinated water molecules (calcd: 3.9%).

$(mimC_{18}H_{37})_{24}[K_2NaLi_3\{Mo_4O_4S_4(OH)_2(H_2O)_3\}_2(H_6P_8W_{48}O_{184})]\cdot 25H_2O$, $(mimC_{18})_{24}$–1. $(mimC_{18}H_{37})_{24}[K_2NaLi_3\{Mo_4O_4S_4(OH)_2(H_2O)_3\}_2(H_6P_8W_{48}O_{184})]\cdot 25H_2O$, **$(mimC_{18})_{24}$–1** was prepared by using **$mimC_{18}Br$** (1.113 g, 2.68 mmol). Yield 385 mg, 98%. IR/cm^{-1}: 3142 (m), 3100 (m), 3078 (m), 2953 (m), 2920 (vs), 2871 (m), 2851 (s), 1635 (w), 1573 (m), 1468 (m), 1166 (m), 1141 (m), 1077 (m), 1017 (w), 938 (s), 882 (mw), 802 (s), 741 (vs). Elemental analysis calcd (%) for $(mimC_{18}H_{37})_{24}[K_2NaLi_3H_6P_8W_{48}O_{184}Mo_8O_8S_8(OH)_4(H_2O)_6]\cdot 25H_2O$ (M = 21 976.9 g mol^{-1}) Li 0.09; Na 0.10; C 28.86; H 5.06; N 3.06; S 1.17. Found: Li 0.09; Na 0.08; C 29.05; H 5.22; N 3.06; S 1.13. EDX atomic ratios calculated for $(mimC_{18}H_{37})_{24}[K_2NaLi_3H_6P_8W_{48}O_{184}Mo_8O_8S_8(OH)_4(H_2O)_6]\cdot 25H_2O$ (found): Mo/S = 1 (1.03); W/Mo = 6 (6.16); W/P = 6 (5.74); Na/K = 0.5 (0.42). TGA: a weight loss of 2.6% between *RT* and 180 °C corresponding to crystallization and coordinated water molecules (calcd: 2.5%).

$(mimC_{20}H_{41})_{24}[K_2NaLi_3\{Mo_4O_4S_4(OH)_2(H_2O)_3\}_2(H_6P_8W_{48}O_{184})]\cdot 15H_2O$, $(mimC_{20})_{24}$–1. $(mimC_{20}H_{41})_{24}[K_2NaLi_3\{Mo_4O_4S_4(OH)_2(H_2O)_3\}_2(H_6P_8W_{48}O_{184})]\cdot 15H_2O$, **$(mimC_{20})_{24}$–1** was prepared by using $mimC_{20}Br$ (1.189 g, 2.68 mmol). Yield 212 mg, 52%. IR/cm^{-1}: 3146 (m), 3103 (m), 3077 (m), 2953 (m), 2920 (vs), 2870 (m), 2851 (s), 1639 (mw), 1572 (m), 1468 (m), 1166 (m), 1138 (m), 1078 (m), 1016 (w), 935 (s), 881 (mw), 800 (s), 720 (vs). Elemental analysis calcd (%) for $(mimC_{20}H_{41})_{24}[K_2NaLi_3H_6P_8W_{48}O_{184}Mo_8O_8S_8(OH)_4(H_2O)_6]\cdot 15H_2O$ (M = 22 470.0 g mol^{-1}) C 30.79; H 5.29; N 2.99; S 1.14. Found: C 30.53; H 5.17; N 2.91; S 1.14. EDX atomic ratios calculated for $(mimC_{20}H_{41})_{24}[K_2NaLi_3H_6P_8W_{48}O_{184}Mo_8O_8S_8(OH)_4(H_2O)_6]\cdot 15H_2O$ (found): Mo/S = 1 (1.12); W/Mo = 6 (5.98); W/P = 6 (6.15); Na/K = 0.50 (0.44). TGA: a weight loss of 1.9% between *RT* and 150 °C corresponding to crystallization and coordinated water molecules (calcd: 1.7%).

$(dmimC_{12}H_{25})_{18}[K_2Na_3Li_5\{Mo_4O_4S_4(OH)_2(H_2O)_3\}_2(H_8P_8W_{48}O_{184})]\cdot 15H_2O$, $(dmimC_{12})_{18}$–1. $(dmimC_{12}H_{25})_{18}[K_2Na_3Li_5\{Mo_4O_4S_4(OH)_2(H_2O)_3\}_2(H_8P_8W_{48}O_{184})]\cdot 15H_2O$, **$(dmimC_{12})_{18}$–1** was prepared by using $dmimC_{12}Br$ (930 mg, 2.68 mmol). Yield 180 mg, 55%. IR/cm^{-1}: 2953 (m), 2925 (vs), 2871 (m), 2853 (s), 1637 (mw), 1588 (w), 1537 (w), 1467 (m), 1240 (w), 1128 (m), 1078 (m), 1016 (w), 932 (s), 880 (mw), 799 (s), 719 (vs). Elemental analysis calcd (%) for $(dmimC_{12}H_{25})_{18}[K_2Na_3Li_5H_8P_8W_{48}O_{184}Mo_8O_8S_8(OH)_4(H_2O)_6]\cdot 15H_2O$ (M = 18 582.6 g mol^{-1}) Li 0.19; Na 0.37; C 19.78; H 3.51; N 2.71; S 1.38. Found: Li 0.22; Na 0.45; C 19.84; H 3.65; N 2.82; S 1.25. EDX atomic ratios calculated for $(dmimC_{12}H_{25})_{18}[K_2Na_3Li_5H_8P_8W_{48}O_{184}Mo_8O_8S_8(OH)_4(H_2O)_6]\cdot 15H_2O$ (found): Mo/S = 1 (1.12); W/Mo = 6 (5.75); W/P = 6 (7.10); Na/K = 1.5 (0.90). TGA: a weight loss of 2.1% between *RT* and 180 °C corresponding to crystallization and coordinated water molecules (calcd: 2.0%).

$(dmimC_{16}H_{33})_{20}[K_2Na_2Li_4\{Mo_4O_4S_4(OH)_2(H_2O)_3\}_2(H_8P_8W_{48}O_{184})]\cdot 20H_2O$, $(dmimC_{16})_{20}$–1. $(dmimC_{16}H_{33})_{20}[K_2Na_2Li_4\{Mo_4O_4S_4(OH)_2(H_2O)_3\}_2(H_8P_8W_{48}O_{184})]\cdot 20H_2O$, **$(dmimC_{16})_{20}$–1** was prepared by using $dmimC_{16}Br$ (1.080 g, 2.68 mmol). Yield 348 mg, 91%. IR/cm^{-1}: 3144 (m), 2956 (m), 2924 (vs), 2872 (m), 2853 (s), 1639 (mw), 1589 (w), 1539 (w), 1466 (m), 1377 (w), 1241 (w), 1142 (m), 1080 (m), 1016 (w), 937 (s), 884 (mw), 808 (s), 721 (vs). Elemental analysis calcd (%) for $(dmimC_{16}H_{33})_{20}[K_2Na_2Li_4H_8P_8W_{48}O_{184}Mo_8O_8S_8(OH)_4(H_2O)_6]\cdot 20H_2O$ (M = 20 316.0 g mol^{-1}) Li 0.14; Na 0.23; C 24.83; H 4.48; N 2.76; S 1.26. Found: Li 0.11; Na 0.27; C 24.82; H 4.62; N 2.79; S 1.19. EDX atomic ratios calculated for $(dmimC_{16}H_{33})_{20}[K_2Na_2Li_4H_8P_8W_{48}O_{184}Mo_8O_8S_8(OH)_4(H_2O)_6]\cdot 20H_2O$ (found): Mo/S = 1 (1.07); W/Mo = 6 (5.73); W/P = 6 (5.94); Na/K = 1 (0.98). TGA: a weight loss of 2.5% in the *RT*–180 °C range corresponding to crystallization and coordinated water molecules (calcd: 2.3%).

Results and discussion

Syntheses and formulae of the POM-based materials

The used precursor $Na_{25}Li[K_2\{Mo_4O_4S_4(OH)_2(H_2O)_3\}_2(H_8P_8W_{48}O_{184})]\cdot 125H_2O$, noted **NaK–1**, corresponds to a P_8W_{48} macrocyclic ring capped on both sides by two cationic molybdenum clusters $[Mo_4O_4S_4(OH)_2(H_2O)_3]^{2+}$. On each side, the $[Mo_4O_4S_4(OH)_2(H_2O)_3]^{2+}$ hemicycles may occupy two equivalent positions, which gives a mixture of two positional isomers characterized by their relative orientation: parallel (noted para, not depicted) or perpendicular (noted perp, depicted in Fig. 1).[31] In this paper, the precursor **NaK–1** mainly contains the perp isomer and the proportion of the two isomers is not further considered.

The POM-based materials are prepared by mixing a 1 M LiCl aqueous solution of **NaK–1** with a $CHCl_3$ solution containing a large excess of organic cations. Due to the red color of the precursor, the transfer of the anionic cluster **1** from the aqueous into the organic phase is easily monitored. It occurs rapidly and quantitatively, and the target materials are selectively precipitated by addition of ethanol into the chloroform phase.

The FT-IR spectra were recorded at room temperature (Fig. S1–S9, ESI†) and some selected stretching vibrations are gathered in the Table 1. Firstly, the FT-IR spectra display the vibration modes of the organic cations associated with the initial cluster **1**, which confirms the integrity of the anionic cluster during the experimental procedure.

EDX, elemental analysis and TGA unambiguously enable establishing the formulae of the POM-based materials. Interestingly, even if a large excess of organic cations is used, the replacement of the alkali cations is not complete. Indeed, the number of organic cations interacting with the anionic

Table 1 Selected IR vibration bands

Compounds	ν_{as} (CH_3)	ν_{as} (CH_2)	ν_s (CH_3)	ν_s (CH_2)	$I(\nu_sCH_2)/I(\nu_{as}CH_2)$
$DODA_{19}$–1	2954	2921	2870	2851	0.81
$(TMAC_{16})_{18}$–1	2955	2924	2871	2853	0.70
$(mimC_{12})_{25}$–1	2954	2923	2870	2852	0.76
$(mimC_{14})_{26}$–1	2955	2920	2871	2851	0.84
$(mimC_{16})_{23}$–1	2954	2919	2871	2850	0.84
$(mimC_{18})_{24}$–1	2953	2920	2871	2851	0.83
$(mimC_{20})_{24}$–1	2953	2920	2870	2851	0.85
$(dmimC_{12})_{18}$–1	2953	2925	2871	2853	0.69
$(dmimC_{16})_{20}$–1	2954	2924	2871	2853	0.74

cluster **1** are found in the 18–26 range, and the residual anionic charges are balanced by protons and residual alkali cations.

The trapping of potassium cations inside the cavity of P_8W_{48} derivatives is commonly observed.[26,32–35] The precursor compound $Na_{25}Li[K_2\{Mo_4O_4S_4(OH)_2(H_2O)_3\}_2(H_8P_8W_{48}O_{184})]\cdot 125H_2O$ contains two potassium cations which are strongly coordinated inside the P_8W_{48} ring. The presence of two potassium cations is found for all materials in this study, which demonstrates their efficient embedding within the cluster **1**. EDX and elemental analysis reveal the presence of 1 to 3 sodium cations and 3 to 6 lithium cations, which also suggest a good affinity of these alkali cations for the cavity of the P_8W_{48} cluster. Finally, 4 to 8 protons are bound to the P_8W_{48} moiety because the pH of the aqueous phase is maintained between 3 and 4.5. To summarize, the cavity of the cluster is filled with alkali cations where as protons are likely localized at the surface P_8W_{48} cluster. The general formulae of the POM based materials can be written as $[K_2Na_xLi_y\{Mo_4O_4S_4(OH)_2(H_2O)_3\}_2(H_zP_8W_{48}O_{184})]^{(34-x-y-z)-}$ (with $1 \leq x \leq 3$, $3 \leq y \leq 6$ and $3 \leq z \leq 8$) together with 18 to 26 organic cations.

When $dmimC_n^+$ (n = 12 and 16) cations are used, the number of cations is significantly lower than that observed in analogous materials incorporating the $mimC_{12}^+$ and $mimC_{16}^+$ cations. This result suggests that (i) the number of organic cations can be modulated by changing the size and the steric hindrance of the imidazolium part of the organic cations and (ii) the organic cations are probably not randomly distributed around the inorganic cluster.

Finally, the amount of water content and the thermal stability of the POM-based materials are assessed by TGA and by variable–temperature FT-IR experiments (see Fig. S10–S21, ESI†). For all materials, a weight loss of 16–46 water molecules per POM–organic assembly occurs in the 25–180 °C range in agreement with the molecular formulae. The decomposition temperatures under an oxygen atmosphere vary as a function of the organic cation from 205 to 235 °C. Higher decomposition temperatures are found under air or under nitrogen. The FT-IR spectra recorded in air in the 20–300 °C temperature range for **$DODA_{19}$–1**, **$(mimC_{16})_{23}$–1** and **$(mimC_{18})_{24}$–1** (see Fig. S10–S12, ESI†) confirm the removal of water molecules in the 20–180 °C range and suggest that the degradation of the materials occurs at temperature above 250 °C.

FT-IR spectroscopies studies

Infrared spectroscopy represents a powerful tool for investigating the organization and dynamics of alkyl chains.[18,20] In the high frequency region, the two weak bands observed about 2953–2955 cm^{-1} and 2870–2871 cm^{-1} can be assigned to the antisymmetric ($\nu_{as}(CH_3)$) and symmetric ($\nu_s(CH_3)$) stretching vibrations of the terminal methyl groups, while the two strong bands found at around 2919–2925 cm^{-1} and 2850–2854 cm^{-1} are assigned to the antisymmetric ($\nu_{as}(CH_2)$) and symmetric ($\nu_s(CH_2)$) stretching vibrations of the methylene groups. These two bands are very useful to study the order of the alkyl chains in the ionic materials. Indeed, low frequencies (2915–2918 and 2846–2850 cm^{-1}) are diagnostic for a highly ordered chain, while their blue shift toward 2924–2928 and 2854–2856 cm^{-1} indicates a larger conformational disorder.[18,20] On the basis of the data reported in Table 1, the alkyl chains of the organic cations found in the compounds **$DODA_{19}$–1**, **$(mimC_{14})_{26}$–1**, **$(mimC_{16})_{23}$–1**, **$(mimC_{18})_{24}$–1**, **$(mimC_{20})_{24}$–1** appear highly ordered even if no thermal treatment has been applied to these materials. On the contrary, the compounds **$(TMAC_{16})_{18}$–1**, **$(dmimC_{12})_{18}$–1**, **$(dmimC_{16})_{20}$–1** seem to be poorly ordered. These data must be correlated to the possible induction of liquid crystal properties for the former compounds whereas the latter does not exhibit any liquid crystal properties (*vide infra*). In the case of **$(mimC_{12})_{25}$–1**, the IR vibration frequencies are intermediate, which suggest this compound to be probably at the boundary between a liquid crystal and solid. In addition, the intensity ratio $I(\nu_s(CH_2))/I(\nu_{as}(CH_2))$ can also be used as an indicator of the alkyl chain arrangement.[18,20] The intensity of this ratio increases when the conformational order of the alkyl chain increases and similar conclusions are obtained. Indeed, as shown in Table 1, mainly two different ranges of values are found for our materials: a "low" ratio in the 0.69–0.74 range for the compounds **$(TMAC_{16})_{18}$–1**, **$(dmimC_{12})_{18}$–1** and **$(dmimC_{16})_{20}$–1** and a "high" ratio in the 0.81–0.85 range for the compounds **$DODA_{19}$–1**, **$(mimC_{14})_{26}$–1**, **$(mimC_{16})_{23}$–1**, **$(mimC_{18})_{24}$–1**, **$(mimC_{20})_{24}$–1**, whereas the **$(mimC_{12})_{25}$–1** exhibits an intermediate value.

The analysis of the position and the intensities of $\nu_{as}(CH_2)$ and $\nu_s(CH_2)$ thus appears as a tool for estimating the potentialities of these materials as liquid crystals. Considering the materials prepared with $mimC_n^+$ cations (n = 12–20), a longer alkyl chain leads to improved van der Waals interactions between the chains and to better organizations.

Finally, in the low frequency region, the absorption bands are mostly composed of the scissoring, wagging, twisting and rocking modes of the CH_2 groups together with the vibration modes of the POM. The vibration bands in the 1483–1466 cm^{-1} are assigned to the $-CH_2-$ scissoring bending modes, which can be used to diagnose alkyl chains packing. Indeed, a single narrow peak at 1473 cm^{-1} is attributed to triclinic subcell packing of alkyl chains, while a single narrow band at 1467 cm^{-1} is typical of a hexagonal subcell.[18,20] The FT-IR spectra of

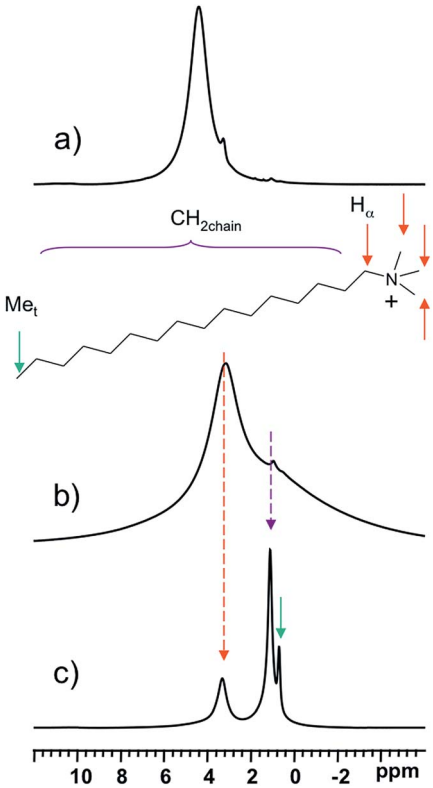

Fig. 2 500.13 MHz ^{1}H NMR spectra at 20 kHz MAS of **NaK–1** (a) trimethylhexadecylammonium chloride (**$TMAC_{16}Cl$**) (b) and **$(TMAC_{16})_{18}$–1** (c). Arrows indicate the assignments of the NMR lines.

our POM-based materials reveal a narrow peak at 1466–1467 cm^{-1}, which is consistent with the tendency of the alkyl chains to give a hexagonal packing arrangement.

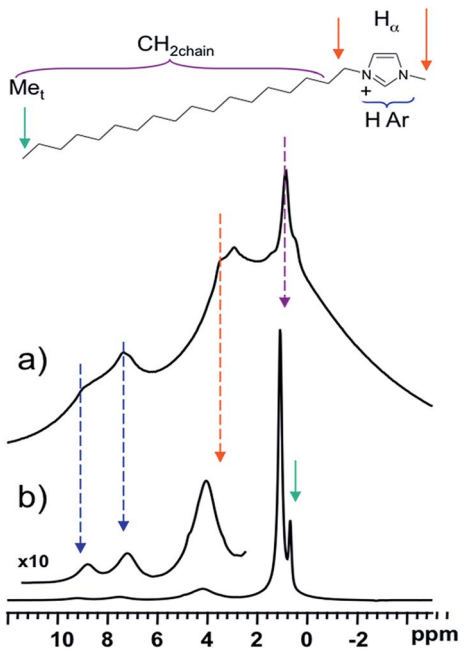

Fig. 3 500.13 MHz ^{1}H NMR spectra at 20 kHz MAS of **$mimC_{18}Br$** (a) and **$(mimC_{18})_{24}$–1** (b). Arrows indicate the assignments of the NMR lines.

NMR studies

^{1}H and ^{31}P NMR studies in solution were performed for the selected compounds **$DODA_{19}$–1**, **$(TMAC_{16})_{18}$–1**, and **$(mimC_{18})_{24}$–1** in $CDCl_3$. Interestingly, the recorded ^{31}P NMR spectra did not exhibit any significant signal. This could be due to some extreme line broadening of the signals caused by the reduced molecular tumbling in the POM–cation assemblies (see Fig. S22–S24 in the ESI†).

Solid state NMR remains underused in the domain of polyoxometalate chemistry although it represents a powerful characterization technique in materials science. This technique was previously used to investigate local structures, interactions between species and some dynamic aspects occurring within the hybrid POM–organic cation assemblies.[36] ^{1}H and ^{13}C NMR are pertinent for probing the organic moiety while ^{31}P NMR is used to investigate the POM part.

Three compounds were considered as representative samples: **$(TMAC_{16})_{18}$–1**, **$DODA_{19}$–1**, and **$(mimC_{18})_{24}$–1**. The ^{1}H NMR spectra of the precursor **NaK–1**, **$(TMAC_{16})_{18}$–1**, **$DODA_{19}$–1**, **$(mimC_{18})_{24}$–1**, and of the corresponding salts **$TMAC_{16}Cl$**, **DODACl**, and **$(mimC_{18})Br$** are shown in Fig. 2–4. The ^{1}H NMR spectrum of **NaK–1** (Fig. 2a) exhibits a main resonance at 4.4 ppm with a shoulder at 3.3 ppm ($\approx$2%) due to water molecules present outside and inside the POM cavity, respectively. In contrast, these NMR signals appear minor in the ^{1}H NMR spectra of **$(TMAC_{16})_{18}$–1**, **$DODA_{19}$–1** and **$(mimC_{18})_{24}$–1** in agreement with the presence of organic cations with dominant signals.

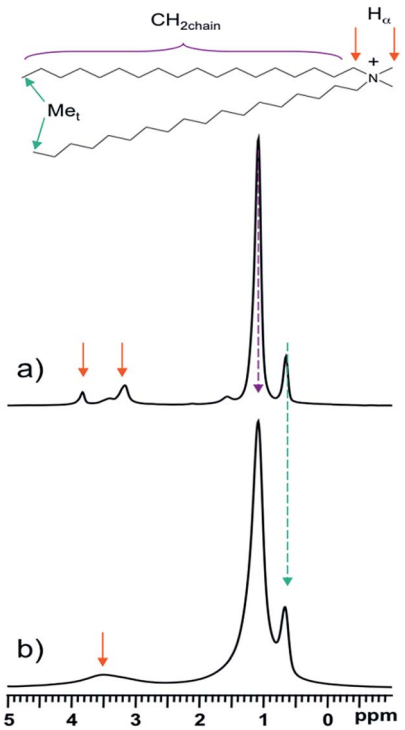

Fig. 4 500.13 MHz ^{1}H NMR spectra at 20 kHz MAS of **DODACl** (a) and **$DODA_{19}$–1** (b). Arrows indicate the assignments of the NMR lines.

The ^{1}H NMR spectrum of **$TMAC_{16}Cl$** (Fig. 2b) consists of two broad resonances at 0.8 and 3.2 ppm corresponding to the protons of the aliphatic chain together with the methyl and methylene groups located close to the ammonium head. The ^{1}H NMR spectrum of the bromide salt **$mimC_{18}Br$** (Fig. 3a) suffers from severe line broadening due to strong H–H dipolar interactions. In contrast, the ^{1}H MAS NMR spectra of their corresponding POM-based materials, **$(TMAC_{16})_{18}$–1** (Fig. 2c and Fig. S25 in the ESI†) and **$(mimC_{18})_{24}$–1** (Fig. 3b) exhibit much narrower signals. For **$(TMAC_{16})_{18}$–1** the NMR spectrum displays three narrower resonances at 0.7, 1.1, and 3.3 ppm due to end-chain methyl group, chain methylene protons, and methylene and methyl groups of the tetraalkylammonium head. For **$(mimC_{18})_{24}$–1**, five resonances assigned to end-chain methyl, chain methylene, N–CH_3/N–CH_2 and aromatic resonances can be distinguished at 0.7, 1.1, 4.3, and 7.6 and 9.2 ppm, respectively. This assignment is supported by ^{13}C{^{1}H} 2D correlation experiments (Fig. S27 and S28, ESI†). The narrowing of the signals for **$(TMAC_{16})_{18}$–1**, and **$(mimC_{18})_{24}$–1** indicates a much lower H–H dipolar interaction. This could be the consequence of a lower density of chain–chain stacking organization in the POM-based materials, which favors chains mobility and increases intermolecular H–H distances.

The reverse situation is observed for **$DODA_{19}$–1**, where the ^{1}H NMR trace shows higher resolution in the chloride salt (Fig. 4). We conclude that the H–H dipolar interaction should be weaker in **DODACl** than in **$DODA_{19}$–1**. The dynamic motions of organic chains in **$DODA_{19}$–1** should be restricted to some extent, and not fast enough to completely average out these interactions. One can therefore deduce that the organic cations are well organized around the POM with a stacking of the aliphatic chains and/or accompanied by strong interdigitation with some neighboring $DODA^{+}$ cations.

The ^{13}C{^{1}H} CPMAS spectra of **$(TMAC_{16})_{18}$–1** and **$DODA_{19}$–1** (Fig. S26 and S29, in ESI†) reveal a narrowing of the NMR lines compared with their halide salts, while the ^{13}C{^{1}H} CPMAS spectrum of **$(mimC_{18})_{24}$–1** (Fig. 5) showed an opposite trend because the resonances are much broader compared with the starting bromide salt. This is consistent with some local disorder in **$(mimC_{18})_{24}$–1**, which produces variable chemical environment around the organic cations. Such a disorder could be explained by the low density of chain–chain staking in the solid state favoring some dynamic motion of these organic chains.

Fig. 6 shows the ^{31}P{^{1}H} MAS spectra of **NaK–1**, **$(TMAC_{16})_{18}$–1**, **$(mimC_{18})_{24}$–1** and **$DODA_{19}$–1**. The precursor **NaK–1** is characterized by a unique resonance at −8.3 ppm consistent with the NMR spectrum recorded in solution (Fig. S30c, ESI†) and characteristic for the presence of the perpendicular isomer as the major species.[31] The spectra of **$(TMAC_{16})_{18}$–1**, **$(mimC_{18})_{24}$–1** and **$DODA_{19}$–1** are comparable to that of the precursor. The spectrum of **$(TMAC_{16})_{18}$–1** shows an asymmetric resonance with a maxima at −7.0 ppm, and a shoulder at −5.5 ppm, while spectra of **$(mimC_{18})_{24}$–1** and **$DODA_{19}$–1** exhibit two main ensembles of composite signals located at *ca.* −6 to −7 and *ca.* −9 ppm. In previous studies, we evidenced that the chemical shift of ^{31}P nuclei of this cluster strongly depended on the nature of the cations trapped within the cavity (see Fig. S30, ESI†).[31] Based on this, the existence of slightly different environments for the ^{31}P nuclei could be explained by a random distribution of K^{+}, Na^{+} and Li^{+} cations within the cavity of the polyoxometalate. This distribution of different sites within the cavity would be at the origin of the

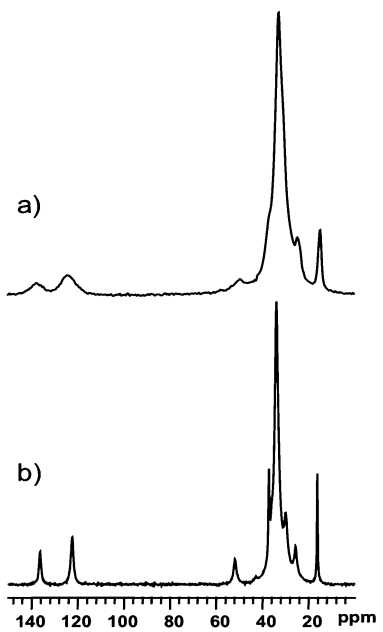

Fig. 5 125.76 MHz ^{13}C{^{1}H} CP NMR spectra at 10 kHz MAS of **$(mimC_{18})_{24}$–1** (a) and **$mimC_{18}Br$** (b).

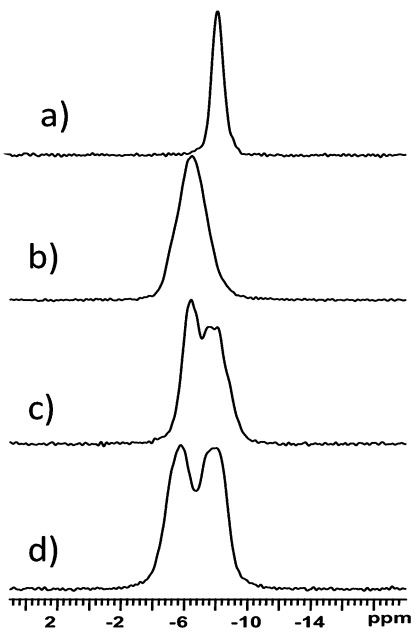

Fig. 6 202.45 MHz ^{31}P{^{1}H} CP NMR spectra at 20 kHz MAS of **NaK–1** (a), **$(TMAC_{16})_{18}$–1** (b), **$(mimC_{18})_{24}$–1** (c), and **$DODA_{19}$–1** (d).

multicomponent resonances visible in the ^{31}P NMR spectra. In summary, these spectra are consistent with the integrity of the polyoxometalate moiety in the materials.

Finally, the ^{31}P{^{1}H} 2D HETCOR experiments performed on **(TMAC$_{16}$)$_{18}$–1**, **(mimC$_{18}$)$_{24}$–1** and **DODA$_{19}$–1** (see Fig. 7) unambiguously evidences specific interactions between the inorganic cluster and the organic cation since a correlation between the ^{31}P nuclei of the cluster and some protons of the organic cations is observed. The major contribution to the ^{1}H to ^{31}P CP transfer arises from the methyl protons of tetraalkylammonium head for **(TMAC$_{16}$)$_{18}$–1**, from the methyl and methylene groups attached to nitrogen atoms of the imidazolium ring for **(mimC$_{18}$)$_{24}$–1**, and from the methyl and methylene groups bound to the ammonium head of DODA^{+} cations for **DODA$_{19}$–1**. These results demonstrate that the polar group of the organic cation interacts with the POM. Wu *et al.* evidenced such an interaction using ^{1}H NMR in solution[19,20,23] and our results indicate that this information can be obtained in the solid state by MAS NMR.

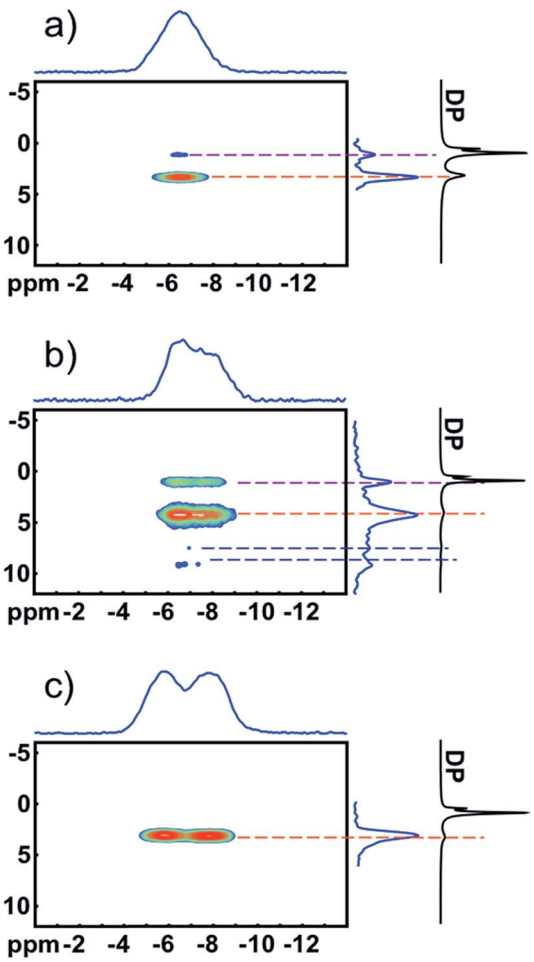

Fig. 7 ^{31}P{^{1}H} HETCOR CPMAS NMR spectra of compounds (TMAC$_{16}$)$_{18}$–1 (a), (mimC$_{18}$)$_{24}$–1 (b), and DODA$_{19}$–1 (c). Projections along ^{1}H and ^{31}P dimensions are shown as well as ^{1}H direct polarization (DP) spectra for comparison purpose.

Liquid crystal properties

The liquid crystal properties of our compounds were studied by Polarized optical microscopy, DSC and SA-XRD during their second heating and cooling process after a first thermal cycle which ensures (i) the removal of water molecules and (ii) the organization of the materials. Mesomorphism in the **DODA$_{19}$–1**, **(mimC$_{12}$)$_{25}$–1**, **(mimC$_{14}$)$_{26}$–1**, **(mimC$_{16}$)$_{23}$–1**, **(mimC$_{18}$)$_{24}$–1**, and **(mimC$_{20}$)$_{24}$–1** materials has been detected by temperature dependent polarized optical microscopy (TD-POM), which revealed the formation of birefringent and homogeneous textures suggesting the liquid-crystalline nature of the samples (Fig. 8). Note that, excepted for **DODA$_{19}$–1**, the fluidity of the compounds **(mimC$_{n}$)$_{x}$–1** is very low and necessitates the use of high temperature to get polarized optical micrograph of good quality. Additionally, in the series of compounds **(mimC$_{n}$)$_{x}$–1**, we logically note that the fluidity of the sample is related to the length of the alkyl chain. In contrast, the three compounds **(TMAC$_{16}$)$_{18}$–1**, **(dmimC$_{12}$)$_{18}$–1**, **(dmimC$_{16}$)$_{20}$–1** did not reveal any liquid crystalline behaviour, thus evidencing the influence of the cationic head on the organization of the materials. Unfortunately, the lack of typical texture due to the decomposition of the cluster before reaching the isotropic state precludes an unambiguous phase assignment by TD-POM.

Differential Scanning Calorimetry (DSC) performed in the −40 °C to 220 °C temperature range (Fig. 9) indicates that mesomorphism occurs after a first-order phase transition in the −3.5 °C to +46.2 °C temperature range (see Table 2) and before the decomposition temperature. It is noteworthy that no first-order phase transition could be observed for **(mimC$_{12}$)$_{25}$–1**. The corresponding melting enthalpy and melting entropy changes, ΔH_m and ΔS_m respectively, are given in Table 2. The

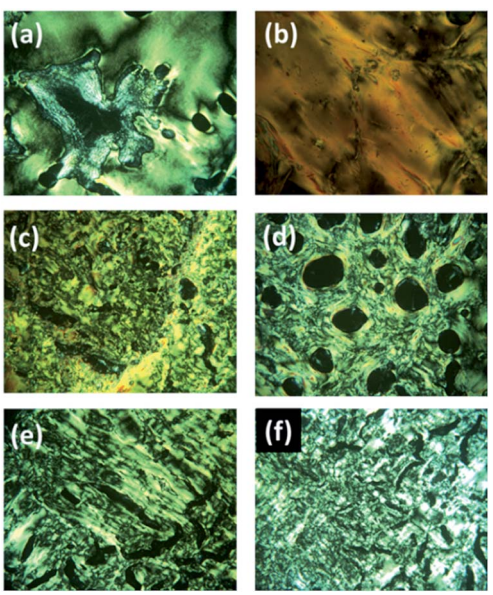

Fig. 8 Polarized optical microphotograph of DODA$_{19}$–1 at 203 °C (a), (mimC$_{12}$)$_{25}$–1 at 240 °C (b), (mimC$_{14}$)$_{26}$–1 at 240 °C (c), (mimC$_{16}$)$_{23}$–1 at 240 °C (d), (mimC$_{18}$)$_{24}$–1 at 240 °C (e) and (mimC$_{20}$)$_{24}$–1 at 240 °C (f).

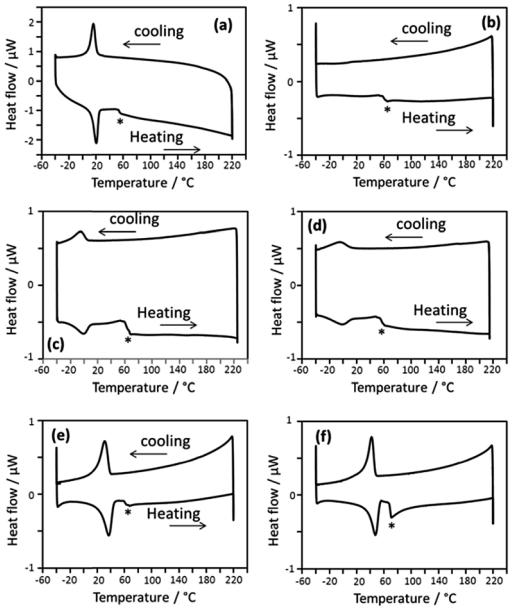

Fig. 9 DSC Traces of the second thermal cycle recorded under N_2 (5 °C min^{-1}) for **$DODA_{19}$–1** (a), **$(mimC_{12})_{25}$–1** (b), **$(mimC_{14})_{26}$–1** (c), **$(mimC_{16})_{23}$–1** (d), **$(mimC_{18})_{24}$–1** (e) and **$(mimC_{20})_{24}$–1** (f). * indicates an unidentified process which has been observed for all samples between 55 and 70 °C during the heating mode. This process does not correspond to a modification of the supramolecular organization and might be attributed to an internal structural change within the clusters core.

straightforward comparison of these values remains difficult. The weighted $\Delta H'_m$ (*i.e.* $\Delta H_m/n\mathrm{CH_2}$) and $\Delta S'_m$ (*i.e.* $\Delta S_m/n\mathrm{CH_2}$) contributions per methylene groups born by the cations in each compound are more informative (see Table 2 and Fig. 10). The plot of $\Delta H'_m$ *versus* $\Delta S'_m$ (Fig. 10) displays a linear relationship typical for *H*/*S* compensation[37] and evidences two sets of points for the materials of this study: **$DODA_{19}$–1**, **$(mimC_{18})_{24}$–1**, and **$(mimC_{20})_{24}$–1** on one hand and **$(mimC_{14})_{26}$–1** and **$(mimC_{16})_{23}$–1** on the other hand, whereas **DODACl** is clearly different. For **DODACl**, the alkyl chains are poorly constrained by the presence of the counter anion Cl^- and the melting of the chains follows the trend expected for simple alkanes.[37] For the three compounds **$DODA_{19}$–1**, **$(mimC_{18})_{24}$–1**, and **$(mimC_{20})_{24}$–1**, the ratios $\Delta H_m/n\mathrm{CH_2}$ and $\Delta S_m/n\mathrm{CH_2}$ are very similar. Taking

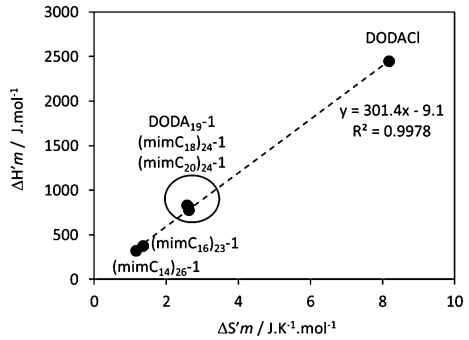

Fig. 10 $\Delta H'_m$ *versus* $\Delta S'_m$ plot.

DODACl as a reference for a "free" alkyl chain, Fig. 10 suggests that the alkyl chains are strongly perturbed by the presence of the bulky P_8W_{48} moieties. From a macroscopic point of view, it results in a drastic lowering of the fluidity of the samples (the fluidity is qualitatively determined by TD-POM). This phenomenon is more pronounced for the two last compounds, **$(mimC_{16})_{23}$–1**, and **$(mimC_{14})_{26}$–1**, which could be better described as soft crystals than as liquid crystals. The magnitude of the $\Delta H_m/n\mathrm{CH_2}$ and $\Delta S_m/n\mathrm{CH_2}$ ratios seems to be strongly and linearly correlated with the average closeness of the $-CH_2-$ with the surface of the anions. In other words, the $-CH_2-$ located closer to the surface are more constrained than those which are more distant. It is as the $-CH_2-$ located in a crown close to the surface were "frozen" and consequently no more available for the melting. In summary, it is the reason why the fluidity of the samples bearing long aliphatic chains is higher.

Temperature dependent Small-Angle X-ray Diffraction (SA-XRD) experiments (−40 °C to 200 °C) were carried out to probe the organization of the liquid crystalline phases. For all compounds, the presence of two, and sometimes three, equidistant reflections in the 1 : 2 (1 : 2 : 3) ratio (indexed as $(00l)$ = (001), (002) and (003)) were detected in the low angle domain (Fig. 11, Table 3, Tables S1–S6 in the ESI†). Such patterns are characteristic for a 1D lamellar ordering. The sharpness of the reflections indicates that they correspond to long range organizations. In addition to the $(00l)$ reflections, a weak reflection called h' is found at $d_{hkl} \approx 22$ Å for at least five of our compounds. This additional reflection is compatible with

Table 2 Temperatures, melting enthalpy and entropy changes of the phase transitions between the glassy state and the lamellar smectic A phase observed for the materials exhibiting liquid crystalline properties. Temperatures are given for the peaks observed by DSC measurements during the second heating process

Cluster	*T*/°C (Heating mode)	ΔH_m/kJ mol^{-1}	ΔS_m/J mol^{-1} K^{-1}	$\Delta H'_m{}^a$/kJ mol^{-1}	$\Delta S'_m{}^a$/J mol^{-1} K^{-1}
$DODA_{19}$–1	+19.7	499.0	1704.1	772.5	2.64
$(mimC_{14})_{26}$–1	−3.0	106.7	395.1	315.8	1.17
$(mimC_{16})_{23}$–1	−3.5	127.0	471.0	368.2	1.37
$(mimC_{18})_{24}$–1	+37.7	330.8	1067.6	813.4	2.62
$(mimC_{20})_{24}$–1	+46.2	375.9	1177.1	823.4	2.58
DODACl	+18.0	83.1	278.5	2445.4	8.19

[a] $\Delta Y'_m = \Delta Y_m/n(\mathrm{CH_2})$ ($Y = H, S$) where $n(\mathrm{CH_2})$ corresponds to the total number of methylene groups of the alkyl chains born by the cations.

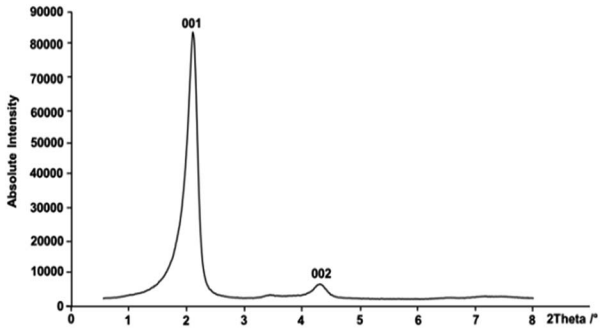

Fig. 11 SA-XRD pattern recorded at 200 °C for compound $(mimC_{16})_{23}$–**1**.

partial 3D structuration, a result in line with the low fluidity of these compounds.[11,24,25] The presence of a broad and diffuse reflection at approximately 4.5 Å associated with the liquid-like molten chains is not observed for our materials, in agreement with the high viscosity of our mesophases. Finally, the absence of any reflection corresponding to intercluster distances implies that clusters are not well organized within the layers. Consequently the liquid crystalline phases behave like smectic A phase (SmA).

Table 3 Indexation at 200 °C during the cooling mode for the reflections detected in the liquid-crystalline phase by SA-XRD. Full data are given in the ESI[a]

Compounds	$d_{hkl(mes)}$/Å	I/a.u.	00l	$d_{hkl(calc)}$/Å	
$DODA_{19}$–1	40.25	VS(Sh)	001	40.33	h = 40.33 Å
	22.54	S(Sh)			h' = 22.54 Å
	20.20	S(Sh)	002	20.16	a_{Hex} = 33.68 Å
	13.5	W(Br)			
	11.4	W(Br)			
$(mimC_{12})_{25}$–1	35.01	VS(Sh)	001	35.15	h = 35.15 Å
	22.15	W(Sh)			h' = 22.15 Å
	17.64	S(Sh)	002	17.57	a_{Hex} = 32.75 Å
	13	W(Br)			
	11	W(Br)			
$(mimC_{14})_{26}$–1	38.39	VS(Sh)	001	38.44	h = 38.14 Å
	22.19	W(Sh)			h' = 22.19 Å
	19.24	S(Sh)	002	19.22	a_{Hex} = 32.10 Å
	13	W(Br)			
	11	W(Br)			
$(mimC_{16})_{23}$–1	41.09	VS(Sh)	001	40.96	h = 40.96 Å
	21.98	—			h' = 21.98 Å
	20.41	S(Sh)	002	20.48	a_{Hex} = 30.97 Å
	12	W(Br)			
$(mimC_{18})_{24}$–1	43.28	VS(Sh)	001	43.28	h = 43.28 Å
	22.37	W(Sh)			h' = 22.37 Å
	21.63	S(Sh)	002	21.64	a_{Hex} = 30.81 Å
	12	W(Br)			
$(mimC_{20})_{24}$–1	45.10	S(Sh)	001	45.03	h = 45.03 Å
	22.48	S(Sh)	002	22.52	a_{Hex} = 30.68 Å
	12	W(Br)			

[a] $d_{hkl(mes)}$ and $d_{hkl(calc)}$ are the measured and calculated diffraction spacing; h is the lattice parameter of the lamellar phase; I corresponds to the intensity of the reflections (VS: very strong, S: strong, W: weak, VW: very weak; br and sh stand for broad and sharp); h and $d_{hkl(calc)}$ are respectively calculated according the formula: $h = 1/2(d_{001(exp)} + 2d_{002(exp)})$ and $d_{hkl(calc)} = h/l$; a_{Hex} is the local hexagonal organization within the layers calculated with eqn (1). The reflection corresponding to the molten aliphatic chains (usually ~4.5 Å) is too broad to be measured.

The lattice parameters h are deduced from the (00l) lines and are found almost constant in the 40–200 °C temperature range (Table 3, Fig. 12a and Tables S1–S6 in the ESI†). This parameter depends on the nature of the organic cations associated with the polyoxometalate. Focusing on the $mimC_n^+$ salts, the plot of the h parameters as a function of the alkyl chain length (Fig. 12b) exhibits a linear relationship with an increase of the h parameter by *ca.* 2.6 Å for successive $mimC_n^+$ and $mimC_{n+2}^+$ salts. This increment is compatible with the distance increase induced by the introduction of two methylene group within an alkyl chain. This result demonstrates (i) that it is possible to easily tune the interlamellar spacing of such a huge inorganic cluster by simply playing with the alkyl chain length of the associated organic cations and (ii) that the interdigitation of the organic cations belonging to two opposite clusters remains necessarily unchanged (it is a full interdigitation), thus leading to a linear expansion of the h parameter with the increasing of the alkyl chains length.

Taking into account a realistic density of $d = 1.0$ g cm^{-3} in the mesophases[11,24,25] and assuming that the clusters are locally packed in a compact hexagonal lattice with one cluster per unit cell ($Z = 1$), we calculate the hexagonal lattice parameters a_{Hex} gathered in Table 3 and which correspond to the average inter-cluster distances. This parameter is minimum for **$(mimC_{20})_{24}$–1** (a_{Hex} = 30.68 Å) and maximum

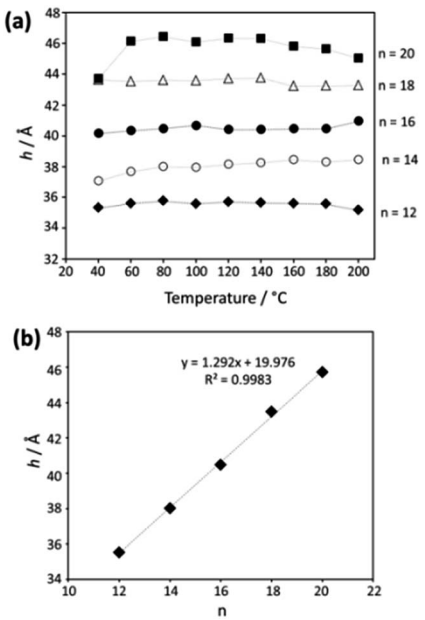

Fig. 12 (a) Variation of the structural parameter h as a function of temperature for compounds $(mimC_n)_x$–**1** (n = 12, 14, 16, 18, 20). (b) Variation of the averaged value of h (in the 20–200 °C temperature range) as a function of alkyl chain length n.

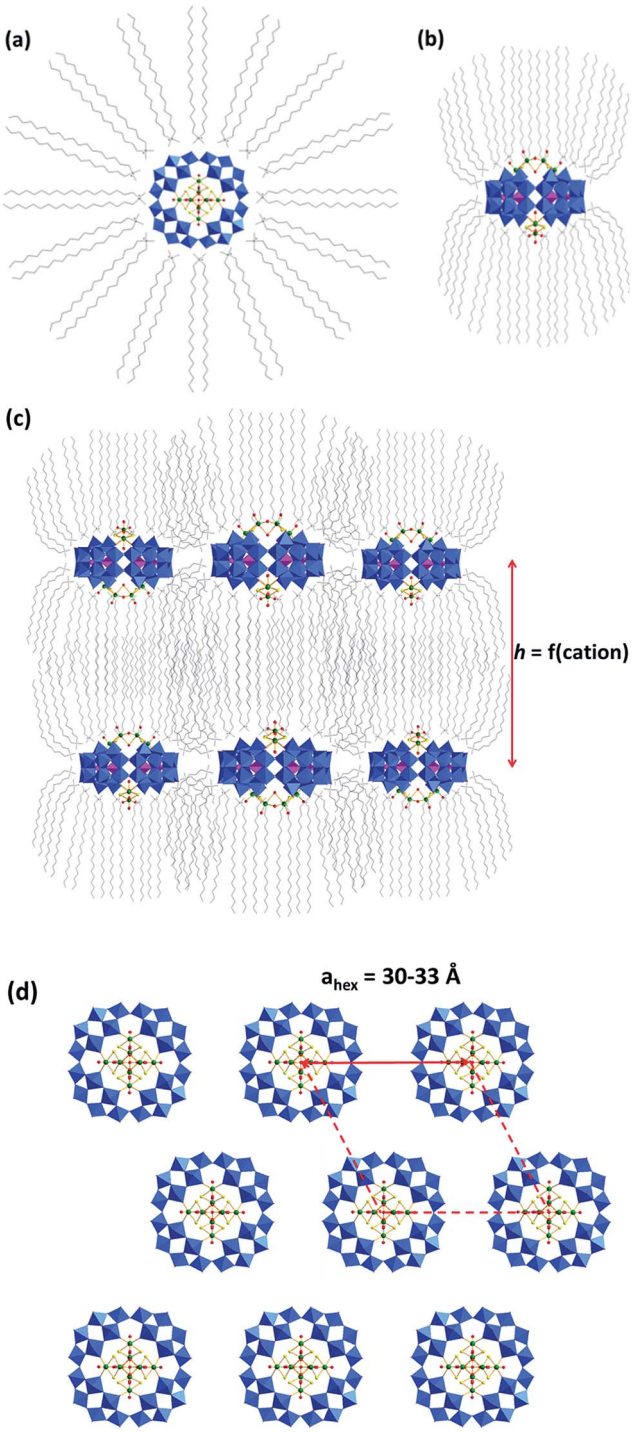

Fig. 13 Schematic representation of the hypothetical organizations of organic cations around the polyanion **1** (a and b); side and top views of the lamellar organization of ionic liquid crystal phases of materials based on the polyanion **1** (c and d). The perp isomer of **1** is mainly taken into account but different position of this isomer should be considered. For the top view, the organic cations are omitted for clarity.

for **DODA$_{19}$–1** (a_{Hex} = 33.89 Å) in the liquid crystalline phase at 200 °C (eqn (1), where N_{AV} is the Avogadro's number, MM_C the molecular weight of the cluster in g mol^{-1}, and h the lamellar periodicity measured by SA-XRD).

$$a_{Hex} = \left(\frac{2ZMM_C}{hdN_{AV} \times 10^{-24} \times 3^{1/2}}\right)^{1/2} \quad (1)$$

The compounds of this study result from the ionic assemblies of DODA$^+$ or mimC$_n^+$ organic cations with the ellipsoidal polyoxometalate anion **1** (diameter ≈ 20.3 Å, thickness ≈ 15.9 Å). As evidenced by solid state NMR, the positive charges of the cations are located close to the negatively charged tungstate groups of the toroidal surface of the P_8W_{48} moiety. They are however not mechanically linked to a specific point of the cluster core. Considering that the values of a_{Hex} do not vary significantly with the nature of the cation, we can rule out the possibility of having the cations aligned along the longer axis as depicted in Fig. 13a and previously reported for $(DODA)_{24}Li[Cu_{20}Cl(OH)_{24}P_8W_{48}O_{184}]\cdot 18H_2O$ in the solid state.[38]

The consideration of a diameter of *ca.* 20 Å with a length of 22 Å for the DODA$^+$ cation, confirms that this hypothesis is not realistic. The only way to make these objects compatible with the values of $30.68 \leq a_{Hex} \leq 33.89$ Å requires that the anchoring sites of the cations are located on the surface of the negatively charged inorganic clusters, whilst the alkyl chains are spread perpendicular to the polyoxometalate macrocycle (Fig. 13b). A related organization is supposed to occur for **(mimC$_n$)$_x$–1** whereas the cations in **(dmimC$_n$)$_x$–1** and **(TMAC$_{16}$)$_{18}$–1** do not display a similar orientation of cations around the POM either due to stronger interactions between the cation and the POM anion or due to sterical constraints between cations. The inorganic cluster shown in the Fig. 13b are packed in the solid state to give the hexagonal lamellar arrangement depicted in Fig. 13c and d. The associated lattice parameters h depend on the alkyl chain length and they are controlled by the thickness of the inorganic cluster (15 Å) and the partial interdigitation of the alkyl chains of the cations. This organization reminds that proposed for Langmuir–Blodgett film obtained for $(DODA)_{24}Li[Cu_{20}Cl(OH)_{24}P_8W_{48}O_{184}]\cdot 18H_2O$.[38] In summary, the ionic associations between the anisotropic POM **1** and organic cations such as DODA$^+$ and a mimC$_n^+$ give lamellar organization, in which the layers are composed of the inorganic clusters and the interlayer spacing is filled by the alkyl chains of the cations.

Conclusion

We prepared a series of new compounds resulting from the ionic association of a nanoscopic inorganic cluster $[K_2Na_xLi_yH_z\{Mo_4O_4S_4(OH)_2(H_2O)_3\}_2(P_8W_{48}O_{184})]^{(34-x-y-z)-}$, denoted **1**, with various organic cations such as DODA$^+$, TMAC$_{16}^+$, mimC$_n^+$ (n = 12–20) and dmimC$_n^+$ (n = 12 and 16). The multinuclear solid state NMR revealed to be a powerful technique for the characterization of these materials and (i) allowed evidencing the strong contacts between the POM and the organic cations and (ii) provided some support for the intermolecular H–H dipolar contacts induced by the interdigitation of the alkyl chains of the cations. For DODA$^+$ and mimC$_n^+$ salts of **1**, Polarized Optical Microscopy, DSC and Small-Angle X-ray diffraction studies revealed ionic liquid crystalline phases of lamellar smectic A type,

even if the fluidity of the $mimC_n^+$ salts is low. These results demonstrate that the strategy which consists by associating highly charged anisotropic polyoxometalate clusters with very simple organic cations bearing only alkyl chains with variable size is efficient to provide finely tuneable liquid crystal phases. Such a strategy allows envisioning the easy preparation of multifunctional materials at a gram scale and the main perspectives for this work aim now at designing materials combining magnetic, optical or trapping properties with liquid crystal behavior.

Acknowledgements

We acknowledge the Centre National de la Recherche Scientifique (CNRS) and the Ministère de l'Education Nationale de l'Enseignement Supérieur et de la Recherche (MENESR) for their financial support. The work was partially supported by RFBR grant 15-33-20651 and by the grant of the President of the Russian Federation SS-516.2014.3.

Notes and references

1 H. J. Lv, Y. V. Geletii, C. C. Zhao, J. W. Vickers, G. B. Zhu, Z. Luo, J. Song, T. Q. Lian, D. G. Musaev and C. L. Hill, *Chem. Soc. Rev.*, 2012, **41**, 7572–7589.

2 B. G. Donoeva, T. A. Trubitsina, G. M. Maksimov, R. I. Maksimovskaya and O. A. Kholdeeva, *Eur. J. Inorg. Chem.*, 2009, 5142–5147.

3 B. Nohra, H. El Moll, L. M. R. Albelo, P. Mialane, J. Marrot, C. Mellot-Draznieks, M. O'Keeffe, R. N. Biboum, J. Lemaire, B. Keita, L. Nadjo and A. Dolbecq, *J. Am. Chem. Soc.*, 2011, **133**, 13363–13374.

4 M. Barsukova-Stuckart, L. F. Piedra-Garza, B. Gautam, G. Alfaro-Espinoza, N. V. Izarova, A. Banerjee, B. S. Bassil, M. S. Ullrich, H. J. Breunig, C. Silvestru and U. Kortz, *Inorg. Chem.*, 2012, **51**, 12015–12022.

5 G. Charron, A. Giusti, S. Mazerat, P. Mialane, A. Gloter, F. Miserque, B. Keita, L. Nadjo, A. Filoramo, E. Rivière, W. Wernsdorfer, V. Huc, J. P. Bourgoin and T. Mallah, *Nanoscale*, 2010, **2**, 139–144.

6 M. D. Symes, P. J. Kitson, J. Yan, C. J. Richmond, G. J. T. Cooper, R. W. Bowman, T. Vilbrandt and L. Cronin, *Nat. Chem.*, 2012, **4**, 349–354.

7 D. L. Long, R. Tsunashima and L. Cronin, *Angew. Chem., Int. Ed.*, 2010, **49**, 1736–1758.

8 E. Terazzi, G. Rogez, J. L. Gallani and B. Donnio, *J. Am. Chem. Soc.*, 2013, **135**, 2708–2722.

9 K. Binnemans and C. Gorller-Walrand, *Chem. Rev.*, 2002, **102**, 2303–2345.

10 N. Tirelli, F. Cardullo, T. Habicher, U. W. Suter and F. Diederich, *J. Chem. Soc., Perkin Trans. 2*, 2000, 193–198.

11 R. Deschenaux, B. Donnio and D. Guillon, *New J. Chem.*, 2007, **31**, 1064–1073.

12 E. Terazzi, S. Suarez, S. Torelli, H. Nozary, D. Imbert, O. Mamula, J. P. Rivera, E. Guillet, J. M. Benech, G. Bernardinelli, R. Scopelliti, B. Donnio, D. Guillon, J. C. G. Bünzli and C. Piguet, *Adv. Funct. Mater.*, 2006, **16**, 157–168.

13 T. Cardinaels, K. Driesen, T. N. Parac-Vogt, B. Heinrich, C. Bourgogne, D. Guillon, B. Donnio and K. Binnemans, *Chem. Mater.*, 2005, **17**, 6589–6598.

14 R. W. Date, E. F. Iglesias, K. E. Rowe, J. M. Elliott and D. W. Bruce, *Dalton Trans.*, 2003, 1914–1931.

15 I. Aprahamian, T. Yasuda, T. Ikeda, S. Saha, W. R. Dichtel, K. Isoda, T. Kato and J. F. Stoddart, *Angew. Chem., Int. Ed.*, 2007, **46**, 4675–4679.

16 Y. Molard, A. Ledneva, M. Amela-Cortes, V. Circu, N. G. Naumov, C. Meriadec, F. Artzner and S. Cordier, *Chem. Mater.*, 2011, **23**, 5122–5130.

17 B. Li, J. Zhang, S. Wang, W. Li and L. X. Wu, *Eur. J. Inorg. Chem.*, 2013, 1869–1875.

18 Y. X. Jiang, S. X. Liu, J. Zhang and L. X. Wu, *Dalton Trans.*, 2013, **42**, 7643–7650.

19 X. K. Lin, W. Li, J. Zhang, H. Sun, Y. Yan and L. X. Wu, *Langmuir*, 2010, **26**, 13201–13209.

20 S. Y. Yin, H. Sun, Y. Yan, W. Li and L. X. Wu, *J. Phys. Chem. B*, 2009, **113**, 2355–2364.

21 W. Li, S. Y. Yin, J. F. Wang and L. X. Wu, *Chem. Mater.*, 2008, **20**, 514–522.

22 W. Li, W. F. Bu, H. L. Li, L. X. Wu and M. Li, *Chem. Commun.*, 2005, 3785–3787.

23 S. Y. Yin, W. Li, J. F. Wang and L. X. Wu, *J. Phys. Chem. B*, 2008, **112**, 3983–3988.

24 S. Floquet, E. Terazzi, V. S. Korenev, A. Hijazi, L. Guénée and E. Cadot, *Liq. Cryst.*, 2014, **41**, 1000–1007.

25 S. Floquet, E. Terazzi, A. Hijazi, L. Guénée, C. Piguet and E. Cadot, *New J. Chem.*, 2012, **36**, 865–868.

26 R. Contant and A. Teze, *Inorg. Chem.*, 1985, **24**, 4610–4614.

27 S. S. Mal, B. S. Bassil, M. Ibrahim, S. Nellutla, J. van Tol, N. S. Dalal, J. A. Fernandez, X. Lopez, J. M. Poblet, R. N. Biboum, B. Keita and U. Kortz, *Inorg. Chem.*, 2009, **48**, 11636–11645.

28 S. S. Mal, M. H. Dickman, U. Kortz, A. M. Todea, A. Merca, H. Bogge, T. Glaser, A. Müller, S. Nellutla, N. Kaur, J. van Tol, N. S. Dalal, B. Keita and L. Nadjo, *Chem.–Eur. J.*, 2008, **14**, 1186–1195.

29 S. Noro, R. Tsunashima, Y. Kamiya, K. Uemura, H. Kita, L. Cronin, T. Akutagawa and T. Nakamura, *Angew. Chem., Int. Ed.*, 2009, **48**, 8703–8706.

30 T. Akutagawa, R. Jin, R. Tunashima, S. Noro, L. Cronin and T. Nakamura, *Langmuir*, 2008, **24**, 231–238.

31 V. S. Korenev, S. Floquet, J. Marrot, M. Haouas, I. M. Mbomekalle, F. Taulelle, M. N. Sokolov, V. P. Fedin and E. Cadot, *Inorg. Chem.*, 2012, **51**, 2349–2358.

32 M. Zimmermann, N. Belai, R. J. Butcher, M. T. Pope, E. V. Chubarova, M. H. Dickman and U. Kortz, *Inorg. Chem.*, 2007, **46**, 1737–1740.

33 S. S. Mal, N. H. Nsouli, M. H. Dickman and U. Kortz, *Dalton Trans.*, 2007, 2627–2630.

34 F. L. Sousa, H. Bogge, A. Merca, P. Gouzerh, R. Thouvenot and A. Müller, *Chem. Commun.*, 2009, 7491–7493.

35 A. Müller, M. T. Pope, A. M. Todea, H. Bögge, J. van Slageren, M. Dressel, P. Gouzerh, R. Thouvenot, B. Tsukerblat and A. Bell, *Angew. Chem., Int. Ed.*, 2007, **46**, 4477–4480.
36 H. El Moll, J. C. Kemmegne-Mbouguen, M. Haouas, F. Taulelle, J. Marrot, E. Cadot, P. Mialane, S. Floquet and A. Dolbecq, *Dalton Trans.*, 2012, **41**, 9955–9963.
37 T. Dutronc, E. Terazzi, L. Guénée, K. L. Buchwalder, A. Spoerri, D. Emery, J. Mareda, S. Floquet and C. Piguet, *Chem.–Eur. J.*, 2013, **19**, 8447–8456.
38 Y. Y. Bao, L. H. Bi, L. X. Wu, S. S. Mal and U. Kortz, *Langmuir*, 2009, **25**, 13000–13006.